

# High quantum-efficiency in lateral PIN photodiode gated by transparent electrode fabricated on SOI film

HAI-QING XIE\*, LI-JUN TANG, JUN-LONG TANG, YONG-JUN WEN

*School of Physics & Electronic Science, Changsha University of Science & Technology, Changsha 410004, P. R. China*

Due to depleted region but not inversion region formed by the gate voltage ( $V_{GK}$ ) in thin film and ITO film with transmittance above 80% at  $\lambda \geq 400\text{nm}$  adopted as transparent electrode, high quantum efficiency (QE) could be achieved in SOI film lateral PIN photodiode gated by transparent electrode (LPIN PD-GTE). Physical models for and analysis for quantum efficiency in LPIN PD-GTE were both presented and validated by ATLAS. Quantum efficiency versus the intrinsic length was also discussed. Results indicated that the QE decreased along with the increasing channel length at  $V_{GK}=0\text{V}$ . However, the contribution of  $V_{GK}$  to QE was larger for longer channel in LPIN PD-GTE. The increasing amplitude were respectively, almost 8% and more than 50% for  $L_f=10\mu\text{m}$  and  $L_f=50\mu\text{m}$  from  $V_{GK}=0\text{V}$  to  $V_{GK}=1.0\text{V}$ . The increment of quantum efficiency in LPIN PD-GTE with  $V_{GK}=0.6\text{V}$  is almost 50% to that in lateral PIN photodiode (LPIN PD) with  $L_f=50\mu\text{m}$  and the same other parameters.

(Received July 26, 2013; accepted January 22, 2014)

*Keywords:* Quantum-efficiency, LPIN PD-GTE, Physical models, Silicon on insulator

## 1. Introduction

In the last few years, fast (gigahertz to tens of gigahertz bandwidth) and responsive photodetectors with low dark current are increasingly needed in optical communication systems and optical storage (OS) systems such as DVD applications [1,2]. Due to high dark current and large capacitor of photodiode and low sensitivity of MOS structure (only one kind of carrier and light-absorption of gate electrode) in CMOS process especially under  $0.25\mu\text{m}$  [3,4], bulk silicon detectors, however, hardly cope with above specifications. Furthermore, high bonding capacitor, cost, and area in bulk silicon detectors limit the ultimate performances of optical receivers' circuits, which becomes a limitation for the deployment of local-area networks, interchip/intrachip interconnects, and for the first mile Ethernet [5].

Thanks to SOI structure which achieves low dark current and parasitic capacitance, monolithic integrated photodetectors with high sensitivity and wide band become possible [6]. Therefore, SOI thin-film lateral PIN photodiodes (LPIN PD) studied by Aryan Afzalian et al are candidates of high interest for short distance optical communication (UV detector) and become the focus for extensive research over the past decade due to its high responsivity and quantum efficiency [7-9]. However, the intrinsic region in LPIN PD, corresponding in fact to P<sup>-</sup>-doping of about  $10^{15}\text{cm}^{-3}$  under actual SOI CMOS processes, can't be fully depleted by lateral reverse bias

compatible with low-voltage operation. In this way, low dark current and high quantum efficiency will be limited due to volume and surface recombination in LPIN PD.

In order to achieve low dark current and high photo-current under low reverse voltage, LPIN PD-GTE based on SOI film compatible with CMOS process was proposed recently. It is verified by physical models and numerical calculations that the LPIN PD-GTE realized high sensitivity and SNR (Signal to Noise Ratio) due to entire intrinsic region vertically depleted by gate voltage [10, 11]. To study the photoelectric characteristics in LPIN PD-GTE furthermore, quantum efficiency in SOI thin film LPIN PD-GTE will be discussed in this paper. Our original models are established and fully validated by ATLAS 2D numerical simulations. Furthermore, comparison of quantum efficiency between LPIN PD-GTE and LPIN-PD with the same process parameters and the influence of process parameters to quantum efficiency in LPIN PD-GTE are also discussed to indicate that the LPIN PD-GTE could be adopted in the target applications with requirement of high responsivity.

## 2. Physical models and analysis

The structure of SOI LPIN PD-GTE was depicted in Fig. 1. The parameters which are compatible with standard  $1\mu\text{m}$  FD SOI CMOS technology were also shown in Fig. 1. The thin Si -film thickness,  $d_{si}$ , is equal to 100nm, the front

oxide thickness,  $d_{FOX}$ , is equal to 10nm, the buried oxide (BOX) thickness,  $d_{BOX}$ , is equal to 380nm and the thickness of substrate,  $d_{sub}$ , is equal to 500nm. The length of the N<sup>+</sup> and P<sup>+</sup> zones,  $L_{PN}$ , is equal to 2 $\mu$ m and  $L_i$ , the length of channel which typically corresponds to P<sup>-</sup>-doping of  $10^{15}\text{cm}^{-3}$ , is equal to five different values, i.e.,  $L_i=10, 20, 30, 40$  and  $50\mu\text{m}$ .

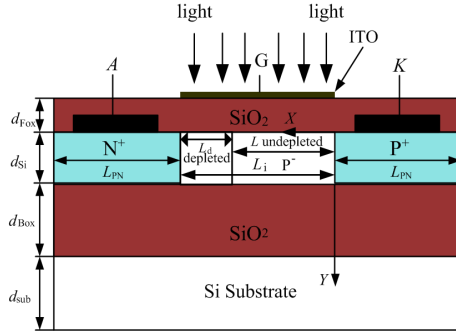


Fig. 1. Schematic cross-section of thin film SOI LPIN PD-GTE.

In LPIN PD-GTE, the efficiency ratio  $\eta = P_{abs} / P_{in}$  strongly depends on  $d_{si}$ , the wavelength of the incident light and the integrated loss due to absorption and reflection over the ray path and is a constant to  $L_i$  [9]. Here,  $P_{in}$  is noted as the optical power density (by unit of area) incidenting vertically to the LPIN PD-GTE, while  $P_{abs}$  is the part absorbed by the device along the thickness ( $d_{si}$ ) of collection area in thin film.

$$P_{abs} = \frac{hc}{\lambda} \int_0^{d_{si}} G(y) dy \quad (1)$$

where  $h$  is Planck's constant,  $c$  is the speed of light,  $\lambda$  is the wavelength,  $G(y)$  is the generation rate given by

$$G(y) = K\alpha e^{-\alpha y} \quad (2)$$

where  $K$  is the internal creating efficiency, which represents the number of carrier pairs generated per one photon absorbed,  $y$  is a relative distance for the ray incident,  $\alpha$  is the absorption coefficient in silicon which is wavelength dependent.

Thus, the mean value of generation rate could be given

$$G_0 = \frac{1}{d_{si}} \int_0^{d_{si}} G(y) = K \cdot [1 - \exp(-\alpha \cdot d_{si})] \quad (3)$$

From above, the absorption in ITO film is the main

loss of incident light. Measurements of transmittance to wavelength of ITO films are presented in Fig. 2. It can be seen that the transmittance of ITO film is higher than 80% for  $\lambda$  above 400nm, and can be adopted as gate electrode in LPIN PD-GTE to reduce light absorption.

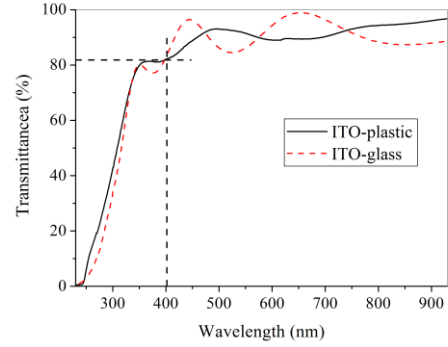


Fig. 2. Transmittance to wavelength of ITO film which was deposited on glass and plastic, respectively, with thickness of 100nm. The deposition of ITO was performed in a vacuum chamber, where the preliminary pressure was  $1 \times 10^{-3} \text{Pa}$ . Sputtering was done at a pressure of 0.5Pa, at a constant power of 100W. During the sputtering process, the temperature of the substrates always was kept at 150  $^{\circ}\text{C}$  for 1.5 hours.

As discussion in Ref [11], lower hole concentration and wider lateral depleted region could be obtained under certain  $V_{AK}$  due to  $V_{GK}$ . In depleted region, volume recombination and surface recombination can be neglected and internal quantum efficiency (QI) is equal to 1. Subsequently, it is important to model the minority carriers' concentration and current density in the undepleted part to achieve quantum efficiency (QE) in LPIN PD-GTE. Due to depleted region but not inversion region formed in thin film by  $V_{GK}$ , the interface potential  $\phi_{sf} \leq 2 \phi_f$  (Femi potential). Therefore, the minority carriers are electrons in LPIN PD-GTE.

From equation (2), the generation term  $G$  is not constant along the depth of the film (the  $y$  direction) and hence, we could expect a variation of the carriers' concentrations in the  $y$  direction. This variation should lead to a diffusive current density in the  $y$  direction,  $J_{ny}$ , to equalize the carrier's concentrations. Thus, the equation to solve for the minority carriers is then [6, 11]

$$\frac{1}{q} \left( \frac{\partial J_{nx}(x, y)}{\partial x} + \frac{\partial J_{ny}(x, y)}{\partial y} \right) + G(y) - \frac{n'(x, y)}{\tau} = 0 \quad (4)$$

where  $n'$  is the excess carriers concentration of electrons and  $\tau$  is their lifetime. Since the thin film is in a

quasi-neutral region due to  $V_{GK}$ , and the lateral voltage  $V_{AK}$  is wholly applied in depleted region, only diffusive currents are assumed in lateral undepleted region. However, electrical field and concentration gradient of electrons both exist at  $y$  direction in the thin film. Subsequently, diffusive currents and drift currents should be both considered at  $y$  direction.

Therefore

$$J_{nx}(x, y) = q \cdot D_n \frac{\partial n'(x, y)}{\partial x} \quad (5)$$

$$J_{ny}(x, y) = q \cdot D_n \frac{\partial n'(x, y)}{\partial y} + q \mu_{ni} n'(x, y) E_y \quad (6)$$

where  $D_n$  is the diffusive coefficient of electron, given by

$$D_n = \mu_{ni} \cdot \varphi_T$$

where  $\mu_{ni}$  is the mobility of electron,  $\varphi_T$  is thermal voltage.

Then, we can split (4) into two equations: one accounting for  $J_{nx}$  and the other for  $J_{ny}$

$$\frac{1}{q} \frac{\partial J_{nx}(x, y)}{\partial x} + G_x(x, y) - \frac{n'(x, y)}{\tau} = 0 \quad (7)$$

$$\frac{1}{q} \frac{\partial J_{ny}(x, y)}{\partial y} + G(y) - G_x(x, y) = 0 \quad (8)$$

where  $G_x(x, y)$  is the part of total optical generation term  $G$  in the  $x$  direction, which will be responsible for  $J_{nx}$ .

Since  $d_{si}$  is very small compared to the diffusive length  $L_{Dn_i}$ , the carriers can diffuse along  $y$  direction without significant recombination in volume. Therefore, we have attributed in equation (3) all volume recombination  $n'(x, y)/\tau$  to  $J_{nx}$  only.

Due to electric field at  $y$  direction,  $G_x(x, y)$  varies with different  $y$  in equation (7). To simplify the calculation, the mean optical generation term is adopted

$$G_x(x) = \frac{1}{d_{si}} \int_0^{d_{si}} G_x(x, y) dy \quad (9)$$

The total number of electrons that have to be

compensated in the  $x$  direction at  $x=x_0$ ,  $N_{G_x(x_0)}$  is equal to  $G_x(x_0) \cdot d_{si}$ . It is equal to the total number of photo-generated electrons  $N_{G_{tot}}$  minus the total number of electrons lost in the  $y$  direction,  $N_{G_y(x_0)}$ , both by volume and surface recombination. Since the volume recombination is negligible in the  $y$  direction,  $N_{G_y(x_0)}$  is equal to the total number of electrons lost by surface recombination at  $x=x_0$ .

In the other way,  $N_{G_y(x_0)}$  is corresponding to the difference between diffusive currents and drift currents at  $y$  direction. Thus,  $N_{G_y(x_0)}$  could be deduced as following.

Using equation (6), equation (8) could be rewritten

$$D_n \frac{\partial^2 n'(x, y)}{\partial y^2} + \mu_{ni} E_y \frac{\partial n'(x, y)}{\partial y} + G(y) - G_x(x, y) = 0 \quad (10)$$

where

$$n'(x, y) = G(y) - s \cdot n'(x) \quad (11)$$

where  $s$  is the volume recombination velocity at  $x$  direction.

From equations (2, 3, 9, 10), we could obtain

$$G_x(x) = G_0 - \frac{(D_n \frac{hc}{\lambda} K\alpha - \mu_{ni} \frac{hc}{\lambda} KE_y) \cdot [1 - \exp(-\alpha \cdot d_{si})]}{d_{si}} - \frac{s \cdot n'(x)}{d_{si}} \quad (12)$$

Thus, using equation (6), equation (7) could be solved

$$D_n \frac{\partial^2 n'(x, y)}{\partial x^2} + G_0 - \frac{(D_n \frac{hc}{\lambda} K\alpha - \mu_{ni} \frac{hc}{\lambda} KE_y) \cdot [1 - \exp(-\alpha \cdot d_{si})]}{d_{si}} - \frac{n'(x, y)}{\tau_{eff}} = 0 \quad (13)$$

where  $\tau_{eff}$  is equivalent lifetime of electron as

$$\frac{1}{\tau_{eff}} = \frac{1}{\tau} + \frac{s}{d_{si}} \quad (14)$$

To solve (13), we have to determine the right boundary conditions for  $x=0$  (the P<sup>+</sup>P boundary) and  $x=L=L_i-L_d$  (undepleted/depleted P<sup>-</sup> boundary). From

discussion above,  $V_{AK}$  was entirely applied to depletion region. At  $x=L$ , using the Maxwell–Boltzmann boundary condition, we get

$$n(x=L) = n_{0i} (e^{V_d/\phi_T} - 1) = n(V_{GK}) (e^{V_d/\phi_T} - 1) \quad (15)$$

For  $x=0$ , the interface of two regions of semiconductor with same type (P) but with different doping levels, like in a pn junction. In order to have the same Fermi levels in the  $P^+$  and  $P^-$  regions, a space charge region and self-built electric field would be obtained. Fortunately, numerical simulations indicate that the width of space charge region is only several nanometers. As depicted in Fig. 3, the electron current density is almost equal to zero at  $x$  and  $y$  directions for  $x=0$ , which indicates the volume recombination at  $x=0$  is approximately equal to zero. Subsequently, the electron concentration at  $x=0$  is the sum of equilibrium electron concentration and generated carriers concentration minus the loss due to interface recombination.

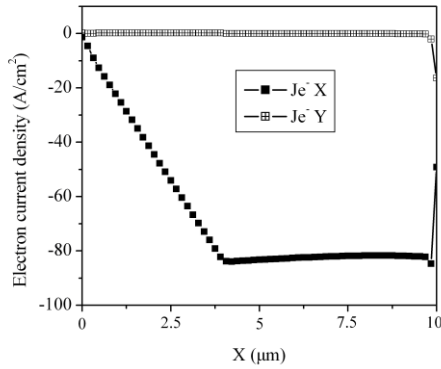


Fig. 3. Lateral electron current density in LPN PD-GTE with  $L_i=20\mu\text{m}$ .

$$\begin{aligned} n(x=0) &= n_{p0} + G_0 - \frac{(D_n K \alpha - \mu_{ni} K E_y) \cdot [1 - \exp(-\alpha \cdot d_{si})]}{d_{si}} \\ &= n(V_{GK}) + G_0 - \frac{(D_n K \alpha - \mu_{ni} K E_y) \cdot [1 - \exp(-\alpha \cdot d_{si})]}{d_{si}} \end{aligned} \quad (16)$$

Thus, equation (13) could be solved

$$n(x) = n(V_{GK}) + G_{0eff} + B_i \cdot \cosh\left(\frac{x}{L_{Dn_i}}\right) \quad (17)$$

where

$$G_{0eff} = G_0 - \frac{(D_n K \alpha - \mu_{ni} K E_y) \cdot [1 - \exp(-\alpha \cdot d_{si})]}{d_{si}} \quad (18)$$

$$B_i = \frac{n(V_{GK}) (e^{V_d/\phi_T} - 1) - G_{0eff}}{\cosh\left(\frac{L}{L_{Dn_i}}\right)} \quad (19)$$

$$L_{Dn_i} = \sqrt{\tau_{eff} \cdot D_n} = \sqrt{\tau_{eff} \cdot \mu_{n_i} \cdot \phi_T} \quad (20)$$

where  $L_{Dn_i}$  is the diffusion length of electrons in the intrinsic region. Here, the  $n(V_{GK})$  is related to  $V_{GK}$ , as described in Ref [11].

Using equation (17), equation (4) could be solved

$$\begin{aligned} J_n(x) &= q \frac{D_n}{L_{Dn_i}} \cdot B_i \cdot \sinh\left(\frac{x}{L_{Dn_i}}\right) \\ &= q \frac{D_n}{L_{Dn_i}} \cdot \frac{n(V_{GK}) (e^{V_d/\phi_T} - 1) - G_{0eff}}{\cosh\left(\frac{L}{L_{Dn_i}}\right)} \cdot \sinh\left(\frac{x}{L_{Dn_i}}\right) \end{aligned} \quad (21)$$

In fact, the carrier's concentration and the current density calculated are the sum of the dark term without illumination ( $G_0=0$ ) and the photogenerated term due to the illumination. Therefore, the photogenerated current density in equation (21) is

$$J_{phn}(x) = -q \frac{D_n \cdot G_{0eff} \cdot \sinh\left(\frac{x}{L_{Dn_i}}\right)}{L_{Dn_i} \cdot \cosh\left(\frac{L}{L_{Dn_i}}\right)} \quad (22)$$

From above, assuming  $QI=1$  for the depletion region, the internal efficiency of the device,  $QI$ , is derived

$$QI = \frac{D_n \cdot G_{0eff} \cdot \tanh\left(\frac{L_i}{L_{Dn_i}}\right)}{L_{Dn_i} \cdot G_0 \cdot L_i} + \frac{L_d}{L_i} \quad (23)$$

Then

$$QE = QI \cdot \frac{P_{abs}}{P_{in}} = QI \cdot \eta \quad (24)$$

### 3. Results and discussions

Numerical simulation studies were conducted by using a two-dimensional (2D) device analysis program (ATLAS by SILVACO, Inc.) implemented on a WINDOWS system [12]. To obtain improved resolution in the regions of interest, the simulation required a very fine mesh in thin film where steep gradients in the electrical field were anticipated. A total of 7599 grid nodes and 14272 elements (triangles) were used in modeling the intermediate length sample ( $L_i=10\mu\text{m}$ ) with a commensurate increase/decrease in the number of nodes and elements for the longer and shorter samples,

respectively. Gummel-Newton-based numerical algorithms were implemented and used by the simulation program in order to solve the discretized form of the field equations [13].

Key parameters of LPIN-PD-GTE in the simulation are listed in Table 1, in which  $N_B$  denotes the acceptor concentration of the silicon substrate,  $N_A$  is the donor concentration of anode region and  $N_K$  is the acceptor

concentration of cathode region.  $N_{ssF}$  and  $N_{ssB}$  are the immobile oxide carrier density per unit of front oxide and back oxide, respectively.  $\tau_n$  and  $\tau_p$ , respectively, are the electron's and hole's lifetimes.  $\mu_n, \mu_p$ , S.N, S.P are mobility of electron and hole, surface recombination velocities of electron and hole, respectively.  $w$  is the width of LPIN PD-GTE.

Table 1. Key parameters of LPIN PD-GTE.

$N_i(\text{cm}^{-3})$	$N_B(\text{cm}^{-3})$	$N_A(\text{cm}^{-3})$	$N_K(\text{cm}^{-3})$	$N_{ssF}(\text{cm}^{-3})$	$N_{ssB}(\text{cm}^{-3})$	$\tau_n$ (s)
$1.45 \times 10^{10}$	$1.0 \times 10^{15}$	$1.0 \times 10^{18}$	$1.0 \times 10^{18}$	$3.0 \times 10^{10}$	$1.0 \times 10^{10}$	$1.0 \times 10^{-7}$
$\tau_p$ (s)	$\mu_n(\text{cm}^2/\text{V}\cdot\text{s})$	$\mu_p(\text{cm}^2/\text{V}\cdot\text{s})$	S.N(cm/s)	S.P(cm/s)	$w$ ( $\mu\text{m}$ )	$\lambda$ (nm)
$1.0 \times 10^{-7}$	1300	491.1	$1.0 \times 10^4$	$1.0 \times 10^4$	50	400

To validate the physical models, numerical calculation results and simulation results are obtained. As shown in Fig. 4, the curve of numerical results for models is well consistent with that of simulation results by ATLAS. However, as ideal lifetime of electron adopted in ATLAS which is different from that used in numerical calculation for models, difference between two curves increases along with increasing channel length.

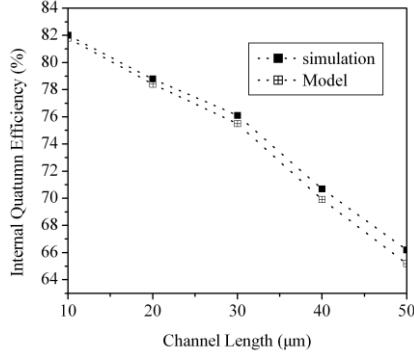


Fig. 4. Curves of numerical calculation for 1-D models and simulation calculation by ATLAS with  $V_{GK}=0.6\text{V}$ ,  $P_{IN}=5\text{mW/cm}^2$ .

From Ref [11], the width of lateral depletion region in LPIN PD-GTE is dominated by  $V_{AK}$  at  $V_{GK}=0$ . At this situation, carriers' concentration in thin film is the same for different channel lengths. In other words, width of lateral depletion region  $L_d$ , lifetime of electrons  $\tau$ , and diffusion length of electrons  $L_{Dn_i}$  are the same for different channel lengths. Thus, from equations (23, 24), QE in LPIN PD-GTE decreases corresponding to increasing channel length. It is worthy for attention, carriers' concentration in thin film decrease with increasing  $V_{GK}$ . Subsequently, width of lateral depletion region  $L_d$ , lifetime of electrons  $\tau$ , and diffusion length of the electrons  $L_{Dn_i}$  increase, and QE also increases.

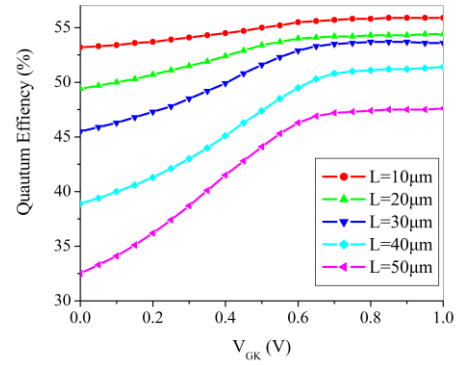


Fig. 5. Curves of quantum efficiency vs.  $V_{GK}$  corresponding to  $L_i=10\mu\text{m}$ ,  $20\mu\text{m}$ ,  $30\mu\text{m}$ ,  $40\mu\text{m}$  and  $50\mu\text{m}$ , respectively.

In addition, the contribution of  $V_{GK}$  to QE is larger for longer channel from equations (23, 24), as shown in Fig. 5. The QE are 53.2% and 32.5% for  $L_i=10\mu\text{m}$  and  $L_i=50\mu\text{m}$ , respectively, at  $V_{GK}=0$ . Whereas, the increasing amplitude are respectively, almost 8% and more than 50% for  $L_i=10\mu\text{m}$  and  $L_i=50\mu\text{m}$  from  $V_{GK}=0\text{V}$  to  $V_{GK}=1.0\text{V}$ . Furthermore, for different channel lengths, obvious differences of QE are obtained from  $V_{GK}=0\text{V}$  to  $V_{GK}=0.6\text{V}$ , whereas, the differences are not discernible from  $V_{GK}=0.6\text{V}$  to  $V_{GK}=1.0\text{V}$ , which is due to weak inversion in thin film under  $V_{GK}$  beyonding 0.6V.

In LPIN PD-GTE, depleted region not inversion region is formed by  $V_{GK}$  in thin film. Subsequently, the lifetime of electrons  $\tau$  and diffusion length of electrons  $L_{Dn_i}$  increase from equation (20). Furthermore, the width of lateral depleted region,  $L_d$  is larger than that in LPIN PD

(without  $V_{GK}$ ). From equation (23), the  $QI$  increases due to increasing  $L_d$  and  $L_{Dn}$ . In addition, with the increasing

channel length  $L_i$ , the influence of  $V_{GK}$  to  $QI$  increases. Although the absorption of ITO will reduce the QE from equation (24), the transmittance of ITO film is over 80% at  $\lambda=400\text{nm}$ , as shown in Fig. 2. Thus, QE of LPIN PD-GTE is higher than that of LPIN PD with the same parameters under certain  $V_{GK}$ . Moreover, with the increasing channel length  $L_i$ , the increment of QE in LPIN PD-GTE to that in LPIN PD increases. As shown in Fig. 6, the QE of LPIN PD-GTE under  $V_{GK}=0.6\text{V}$  is almost 50% increment to that of LPIN-PD with  $L_i=50\mu\text{m}$ .

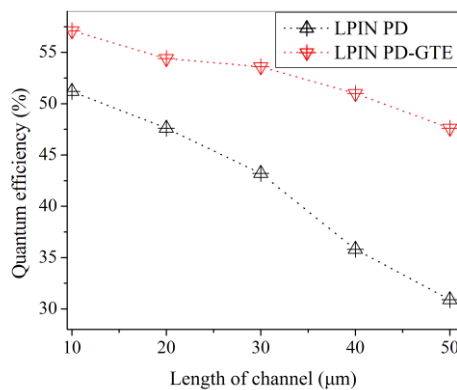


Fig. 6. Comparison of quantum efficiencies between LPIN PD-GTE under  $V_{GK}=0.6\text{V}$  and LPIN-PD with the same parameters.

#### 4. Conclusion

In LPIN PD-GTE, thin film is depleted by  $V_{GK}$  to decrease carriers' concentration. Therefore, wider lateral depletion region  $L_d$  and longer diffusion length of electrons  $L_{Dn}$  could be obtained under certain  $V_{AK}$  than that at  $V_{GK}=0\text{V}$ . In addition, ITO film with transmittance over 80% at  $\lambda=400\text{nm}$  is adopted as gate electrode in LPIN PD-GTE. Physical models of QE in LPIN PD-GTE are presented and numerical simulations are carried out by ATLAS. Results indicate that QE of LPIN PD-GTE decreases along with increasing channel length at certain  $V_{GK}$ . Whereas, the contribution of  $V_{GK}$  to QE is discernible with increasing channel length. From  $V_{GK}=0\text{V}$  to  $V_{GK}=1.0\text{V}$ , the increasing amplitude are respectively, almost 8% and more than 50% for  $L_i=10\mu\text{m}$  and  $L_i=50\mu\text{m}$ . It is worthy for attention, the QE in LPIN PD-GTE with  $V_{GK}=0.6\text{V}$  is almost 50% increment to that in LPIN PD with  $L_i=50\mu\text{m}$  and the same other parameters. All these indicate that LPIN PD-GTE is very advantageous for

application in sensitive optical storage or communication systems.

#### Acknowledgment

This work was supported by the Scientific Research Fund of Hunan Provincial Education Department (Grant No. 12C0043), the construct program of the key discipline in Hunan province, and Aid program for Science and Technology Innovative Research Team in Higher Educational Institutions of Hunan Province.

#### References

- [1] S. Csutak, J. Schaub, W. Wu, et al. IEEE J. Quantum Electron, **38**(2), 193 (2002).
- [2] M. Ghioni, F. Zappa, V. P. Kesan et al. IEEE Trans. Electron Devices, **43**(7), 1054 (1996).
- [3] H. S. Wong, Y. Heights, IEEE Trans. Electron Devices, **43**(12), 2131 (1996).
- [4] N. H. Zhu, Y. Liu, S. J. Zhang, et al. Microwave and Optical Technology Letters, **48**(1), 76 (2006).
- [5] F. A. Mendonça, R. V. Ramos, Microwave and Optical Technology Letters, **45**(5), 415 (2005).
- [6] D. Flandre, J. P. Colinge, J. Chen et al. Analog Integrated Circuits and Signal Processing, **21**(3), 213 (1999).
- [7] A. Afzalian, D. Flandre, IEEE Trans. Electron Device, **52**(6), 1116 (2005).
- [8] A. Afzalian, D. Flandre, IEEE Electron Letter, **42**(24), 1420 (2006).
- [9] A. Afzalian, D. Flandre, Solid-State Electronics, **51**, 337 (2007).
- [10] Y. Zeng, H. Q. Xie, W. Q. Huang, et al. Optics and Photonics Letters, **2**(1), 15 (2009).
- [11] H. Q. Xie, Y. Zeng, J. P. Zeng, et al. Journal of Central South University of Technology, **18**(3), 744 (2011).
- [12] ATLAS Users Manual. SILVACA, Inc., Santa Clara, CA, 2003.
- [13] A. T. Hatzopoulos, N. Arpatzianis, D. H. Tassis, et al. J. Appl. Phys, **100**(11), 114311-114311-7 (2006).

\*Corresponding author: xiehaiqing@gmail.com, xhq\_108@163.com